PLOS ONE

RESEARCH ARTICLE

A revised model for Jeffrey nanofluid subject to convective condition and heat generation/ absorption

Tasawar Hayat[1,2], Arsalan Aziz[1], Taseer Muhammad[1]*, Ahmed Alsaedi[2]

1 Department of Mathematics, Quaid-I-Azam University, Islamabad, Pakistan, **2** Nonlinear Analysis and Applied Mathematics (NAAM) Research Group, Department of Mathematics, Faculty of Science, King Abdulaziz University, Jeddah, Saudi Arabia

* taseer_qau@yahoo.com

Abstract

Here magnetohydrodynamic (MHD) boundary layer flow of Jeffrey nanofluid by a nonlinear stretching surface is addressed. Heat generation/absorption and convective surface condition effects are considered. Novel features of Brownian motion and thermophoresis are present. A non-uniform applied magnetic field is employed. Boundary layer and small magnetic Reynolds number assumptions are employed in the formulation. A newly developed condition with zero nanoparticles mass flux is imposed. The resulting nonlinear systems are solved. Convergence domains are explicitly identified. Graphs are analyzed for the outcome of sundry variables. Further local Nusselt number is computed and discussed. It is observed that the effects of Hartman number on the temperature and concentration distributions are qualitatively similar. Both temperature and concentration distributions are enhanced for larger Hartman number.

Citation: Hayat T, Aziz A, Muhammad T, Alsaedi A (2017) A revised model for Jeffrey nanofluid subject to convective condition and heat generation/absorption. PLoS ONE 12(2): e0172518. doi:10.1371/journal.pone.0172518

Editor: Zhong-Ke Gao, Tianjin University, CHINA

Received: July 14, 2016

Accepted: February 6, 2017

Published: February 23, 2017

Data Availability Statement: All relevant data are within the paper.

Funding: The author(s) received no specific funding for this work.

Competing interests: The authors have declared that no competing interests exist.

1. Introduction

The mixture of ultrafine nanometer sized particles and a convectional heat transfer base fluid is known as nanofluid. These nanometer sized particles have different physical and chemical characteristics. Such particles have thermal conductivities remarkably higher than base liquids. The prime use of nanofluids is for thermal conductivity improvement. Nanofluids are significant in various applications including paper and printing, paints and coatings, power generation, drug delivery, cancer therapy, ceramics and food products etc. Further magneto nanofluids are quite prevalent in MHD pumps and accelerators, hyperthermia, cancer tumor treatment, sink float separation, wound treatment and several others. Choi and Eastman [1] proposed the word nanofluid. They concluded that insertion of metallic nanoparticles in the ordinary fluids can dramatically enhance the thermal conductivities and improve the heat transfer performance of these fluids. A model for convective transport in nanofluids was presented by Buongiorno [2]. He pointed out that Brownian diffusion and thermophoresis are the most important slip mechanisms. Boundary layer flow of nanofluid induced by a linear stretching surface was discussed by Khan and Pop [3]. Turkyilmazoglu and Pop [4] examined

unsteady natural convection flow of nanofluids by a vertical flat plate with radiation. Double stratification effect in boundary-layer flow of nanofluid by a vertical plate is reported by Ibrahim and Makinde [5]. Further relevant studies involving nanofluids can be seen through the investigations [6–25] and various studies therein.

The study of boundary layer flow caused by a stretchable surface is relevant in numerous industrial and engineering utilizations. Such applications include drawing of copper wires, condensation process, die forging and extrusion of polymer in melt spinning, polymer extrusion, continuous stretching of plastic films, metal extrusion, paper production and fiber production etc. It is noted that stretching of surface is not linear in all the cases. The stretching surface may be nonlinear. Gupta and Gupta [26] declared that the stretching of surface is not linear in plastic process. Vajravelu [27] addressed two-dimensional flow of viscous fluid over a nonlinear stretching surface. Here power law surface velocity distribution $u_w(x) = cx^n$ is considered. Cortell [28] analyzed heat transfer in the flow past a nonlinear stretching surface. Here two different thermal boundary conditions on the surface namely constant surface temperature and prescribed surface temperature are employed. The boundary layer flow of viscous fluid induced by a nonlinear stretching surface with thermal radiation and viscous dissipation effects is addressed by Cortell [29]. Hydromagnetic flow generated by a nonlinear stretching surface through modified Adomian decomposition method and Pade approximation technique is demonstrated by Hayat et al. [30]. Rana and Bhargava [31] studied flow of nanofluid over a nonlinear stretching surface with heat transfer. Mukhopadhyay [32] addressed the flow and heat transfer characteristics in the flow of nanofluid over a permeable nonlinear stretching surface with partial slip condition. Mustafa et al. [33] explored axisymmetric flow of nanofluid over a nonlinear stretching surface. Magnetohydrodynamic flow of water-based nanofluid bounded by a nonlinear stretching surface with viscous dissipation is analyzed by Mabood et al. [34]. Magnetohydrodynamic flow of second grade nanofluid over a nonlinear stretching surface is reported by Hayat et al. [35].

Recently the non-Newtonian fluids have gained much attention due to their extensive industrial and engineering applications. These applications involve bioengineering and polymeric liquids, plastics manufacturing, food processing, petroleum production, annealing and thinning of copper wires, drawing of stretching sheet through quiescent fluid, aerodynamic extrusion of plastic films etc. The Navier-Stokes equations are not appropriate to characterize the flow of non-Newtonian fluids. A single relation is not sufficient to predict the characteristics of all the non-Newtonian materials. Therefore different types of relations are given in the literature. The fluid model under discussion is called Jeffrey material [36–41]. This model is linear viscoelastic fluid which exhibits the effects of ratio of relaxation to retardation times and retardation time. The Jeffrey fluid is a relatively simpler linear model considering time derivatives while in non-Newtonian fluid mechanics convective derivatives are assumed. Further the analysis of liquid-liquid two-phase flows are widely encountered in several industrial processes such as spray processes, lubrication, natural gas networks, nuclear reactor cooling etc. Thus Gao et al. [42] provided a multivariate weighted complex network analysis to characterize the nonlinear dynamic behavior in two-phase flow. Gao et al. [43] also addressed the multi-frequency complex network to uncover oil-water flows. Slug to churn flow transition with multivariate pseudo Wigner distribution and multivariate multiscale entropy is reported by Gao et al. [44]. Recently Gao et al. [45] provided a four-sector conductance method to explore the low-velocity oil-water two-phase flows.

Present communication explores magnetohydrodynamic (MHD) boundary-layer flow of Jeffrey nanofluid over a nonlinear stretching surface. Jeffrey fluid is assumed to be electrically conducting. We considered the simultaneous effects of heat and mass transfer in the presence of Brownian motion, thermophoresis and heat generation/absorption. Thermal convective

[46, 47] and zero nanoparticles mass flux [48, 49] conditions are imposed at the stretching surface. These conditions are studied rarely and more realistic physically. To the best of our knowledge, no such consideration for the flow of Jeffrey nanofluid is made yet. Small magnetic Reynolds number and boundary layer are used in mathematical modelling. The governing nonlinear ordinary differential equations are solved by homotopy analysis method (HAM) [50–60]. This technique for the solutions development has advantages through three directions i.e., (i) It is independent of small/large physical parameters. (ii) It provides a simple way to ensure the convergence of series solutions. (iii) It provides freedom to choose the base functions and related auxiliary linear operators. Temperature and concentration profiles are examined via plots. The local Nusselt number is computed numerically and analyzed.

2. Statement

Two-dimensional (2D) flow of Jeffrey nanofluid induced by a surface stretching with nonlinear velocity is considered. Non-uniform magnetic field of strength B_0 acts in the $y-$ direction. Small magnetic Reynolds number justifies the absence of induced magnetic field. Non-uniform heat generation/absorption effect is considered. Brownian motion and thermophoresis are present. The $x-$ and $y-$ axes are along and transverse to the surface respectively. The stretching velocity is $u_w(x) = ax^n$ ($a, n > 0$). The surface temperature is regulated by a convective heating process which is described by heat transfer coefficient h_f and temperature of hot fluid T_f under the surface. Resulting boundary layer problems are

$$\frac{\partial u}{\partial x}+\frac{\partial v}{\partial y}=0, \tag{1}$$

$$u\frac{\partial u}{\partial x}+v\frac{\partial u}{\partial y}=\frac{\nu}{1+\lambda_1}\left(\frac{\partial^2 u}{\partial y^2}+\lambda_2\left(u\frac{\partial^3 u}{\partial x\partial y^2}-\frac{\partial u}{\partial x}\frac{\partial^2 u}{\partial y^2}+\frac{\partial u}{\partial y}\frac{\partial^2 u}{\partial x\partial y}+v\frac{\partial^3 u}{\partial y^3}\right)\right)-\frac{\sigma B^2(x)}{\rho_f}u, \tag{2}$$

$$u\frac{\partial T}{\partial x}+v\frac{\partial T}{\partial y}=\alpha\frac{\partial^2 T}{\partial y^2}+\frac{(\rho c)_p}{(\rho c)_f}\left(D_B\left(\frac{\partial T}{\partial y}\frac{\partial C}{\partial y}\right)+\frac{D_T}{T_\infty}\left(\frac{\partial T}{\partial y}\right)^2\right)+\frac{Q(x)}{(\rho c)_f}(T-T_\infty), \tag{3}$$

$$u\frac{\partial C}{\partial x}+v\frac{\partial C}{\partial y}=D_B\left(\frac{\partial^2 C}{\partial y^2}\right)+\frac{D_T}{T_\infty}\left(\frac{\partial^2 T}{\partial y^2}\right), \tag{4}$$

$$u=u_w(x)=ax^n,\ \ v=0,\ \ -k\frac{\partial T}{\partial y}=h_f(T_f-T),\ \ D_B\frac{\partial C}{\partial y}+\frac{D_T}{T_\infty}\frac{\partial T}{\partial y}=0 \text{ at } y=0, \tag{5}$$

$$u\to 0,\quad T\to T_\infty,\quad C\to C_\infty\ \ \text{as } y\to\infty. \tag{6}$$

Note that u and v depict the flow velocities in the horizontal and vertical directions respectively while ν ($=\mu/\rho_f$), μ and ρ_f show the kinematic viscosity, dynamic viscosity and density of base liquid respectively. The ratio of relaxation to retardation times and the retardation time are represented by λ_1 and λ_2. Here σ represents the electrical conductivity, $B(x)=B_0x^{\frac{n-1}{2}}$ the non-uniform magnetic field, T the temperature, $\alpha = k/(\rho c)_f$, k, $(\rho c)_f$ and $(\rho c)_p$ the thermal diffusivity, thermal conductivity, heat capacity of liquid and effective heat capacity of nanoparticles respectively, $Q(x)=Q_0x^{n-1}$ the non-uniform heat generation/absorption coefficient, D_B the Brownian diffusivity, C the concentration, D_T the thermophoretic diffusion coefficient, a the positive constant and T_∞ and C_∞ the ambient fluid temperature and concentration

respectively. Putting

$$\left.\begin{aligned} u = ax^n f'(\zeta),\ v = -\left(\frac{av(n+1)}{2}\right)^{1/2}(x)^{\frac{n-1}{2}}\{f(\zeta)+\frac{n-1}{n+1}\zeta f'(\zeta)\},\\ \theta(\zeta)=\frac{T-T_\infty}{T_f-T_\infty},\ \phi(\zeta)=\frac{C-C_\infty}{C_\infty},\ \zeta=\left(\frac{a(n+1)}{2v}\right)^{1/2}(x)^{\frac{n-1}{2}}y, \end{aligned}\right\} \tag{7}$$

Eq (1) is trivially satisfied while Eqs (2)–(6) are reduced to

$$\begin{aligned} &f''' + \beta_1\left(\left(\frac{3n-1}{2}\right)(f'')^2 - \left(\frac{n+1}{2}\right)ff'''' + (n-1)ff''\right)\\ &+(1+\lambda_1)\left(ff'' - \left(\frac{2n}{n+1}\right)(f')^2 - \left(\frac{2}{n+1}\right)(Ha)^2 f'\right) = 0, \end{aligned} \tag{8}$$

$$\theta'' + \Pr(f\theta' + N_b\theta'\phi' + N_t\theta'^2 + \left(\frac{2}{n+1}\right)S_1\theta) = 0, \tag{9}$$

$$\phi'' + Le\Pr f\phi' + \frac{N_t}{N_b}\theta'' = 0, \tag{10}$$

$$f = 0,\ f' = 1,\ \theta' = -\gamma(1-\theta(0)),\ N_b\phi' + N_t\theta' = 0 \text{ at } \zeta = 0, \tag{11}$$

$$f' \to 0,\ \theta \to 0,\ \phi \to 0 \text{ when } \zeta \to \infty. \tag{12}$$

Here β_1 denotes local Deborah number, Ha Hartman number, γ Biot number, S_1 heat generation/absorption parameter, Pr Prandtl number, N_b Brownian motion parameter, N_t thermophoresis parameter and Le Lewis number. The definitions of these parameters are

$$\left.\begin{aligned} \beta_1 = \lambda_2 a x^{n-1},\ (Ha)^2 = \frac{\sigma B_0^2}{a\rho_f},\ \gamma = \frac{h_f}{k}\sqrt{\frac{v}{a}},\ S_1 = \frac{Q_0}{a(\rho c)_f}\\ N_b = \frac{(\rho c)_p D_B C_\infty}{(\rho c)_f v},\ N_t = \frac{(\rho c)_p D_T(T_f - T_\infty)}{(\rho c)_f v T_\infty},\ Le = \frac{\alpha}{D_B},\ \Pr = \frac{v}{\alpha}. \end{aligned}\right\} \tag{13}$$

Local Nusselt number is given by

$$Re_x^{-1/2}Nu_x = -\left(\frac{n+1}{2}\right)^{1/2}\theta'(0). \tag{14}$$

The non-dimensional local Sherwood number is identically zero and $\mathrm{Re}_x = u_w x/v$ represents the local Reynolds number.

3. Solutions by HAM

The appropriate initial approximations and auxiliary linear operators for approximate series solutions by homotopy analysis method (HAM) are

$$f_0(\zeta) = 1 - e^{-\zeta}, \quad \theta_0(\zeta) = \frac{\gamma}{1+\gamma} e^{-\zeta}, \quad \phi_0(\zeta) = -\frac{\gamma}{1+\gamma}\frac{N_t}{N_b} e^{-\zeta}, \tag{15}$$

$$\mathbf{L}_f = \frac{d^3 f}{d\zeta^3} - \frac{df}{d\zeta}, \quad \mathbf{L}_\theta = \frac{d^2\theta}{d\zeta^2} - \theta, \quad \mathbf{L}_\phi = \frac{d^2\phi}{d\zeta^2} - \phi, \tag{16}$$

subject to

$$\mathbf{L}_f[B_1^* + B_2^* e^{\zeta} + B_3^* e^{-\zeta}] = 0, \ \mathbf{L}_\theta[B_4^* e^{\zeta} + B_5^* e^{-\zeta}] = 0, \ \mathbf{L}_\phi[B_6^* e^{\zeta} + B_7^* e^{-\zeta}] = 0, \tag{17}$$

where B_j^* (j = 1–7) denote the arbitrary constants. Deformation problems at zeroth-order are

$$(1-\text{þ})\mathbf{L}_f[\breve{f}(\zeta,\text{þ}) - f_0(\zeta)] = \text{þ}\hbar_f \mathbf{N}_f[\breve{f}(\zeta,\text{þ})], \tag{18}$$

$$(1-\text{þ})\mathbf{L}_\theta[\breve{\theta}(\zeta,\text{þ}) - \theta_0(\zeta)] = \text{þ}\hbar_\theta \mathbf{N}_\theta[\breve{f}(\zeta,\text{þ}), \breve{\theta}(\zeta,\text{þ}), \breve{\phi}(\zeta,\text{þ})], \tag{19}$$

$$(1-\text{þ})\mathbf{L}_\phi[\breve{\phi}(\zeta,\text{þ}) - \phi_0(\zeta)] = \text{þ}\hbar_\phi \mathbf{N}_\phi[\breve{f}(\zeta,\text{þ}), \breve{\theta}(\zeta,\text{þ}), \breve{\phi}(\zeta,\text{þ})], \tag{20}$$

$$\begin{gathered}\breve{f}(0,\text{þ}) = 0, \ \breve{f}'(0,\text{þ}) = 1, \ \breve{f}'(\infty,\text{þ}) = 0, \ \breve{\theta}'(0,\text{þ}) = -\gamma(1-\breve{\theta}(0,\text{þ})), \\ \breve{\theta}(\infty,\text{þ}) = 0, \ Nb\breve{\phi}'(0,\text{þ}) + Nt\breve{\theta}'(0,\text{þ}) = 0, \ \breve{\phi}(\infty,\text{þ}) = 0,\end{gathered} \tag{21}$$

$$\begin{aligned}\mathbf{N}_f[\breve{f}(\zeta;\text{þ})] = \frac{\partial^3\breve{f}}{\partial\zeta^3} + \beta_1\left(\left(\frac{3n-1}{2}\right)\left(\frac{\partial^2\breve{f}}{\partial\zeta^2}\right)^2 - \left(\frac{n+1}{2}\right)\breve{f}\frac{\partial^4\breve{f}}{\partial\zeta^4} + (n-1)\breve{f}\frac{\partial^3\breve{f}}{\partial\zeta^3}\right) \\ +(1+\lambda_1)\left(\breve{f}\frac{\partial^2\breve{f}}{\partial\zeta^2} - \left(\frac{2n}{n+1}\right)\left(\frac{\partial\breve{f}}{\partial\zeta}\right)^2 - \left(\frac{2}{n+1}\right)(Ha)^2\frac{\partial\breve{f}}{\partial\zeta}\right),\end{aligned} \tag{22}$$

$$\mathbf{N}_\theta[\breve{f}(\zeta;\text{þ}), \breve{\theta}(\zeta,\text{þ}), \breve{\phi}(\zeta,\text{þ})] = \frac{1}{\Pr}\frac{\partial^2\breve{\theta}}{\partial\zeta^2} + \breve{f}\frac{\partial\breve{\theta}}{\partial\zeta} + N_b\frac{\partial\breve{\theta}}{\partial\zeta}\frac{\partial\breve{\theta}}{\partial\zeta} + N_t\left(\frac{\partial\breve{\theta}}{\partial\zeta}\right)^2 + \left(\frac{2}{n+1}\right)S_1\breve{\theta}, \tag{23}$$

$$\mathbf{N}_\phi[\breve{f}(\zeta;\text{þ}), \breve{\theta}(\zeta,\text{þ}), \breve{\phi}(\zeta,\text{þ})] = \frac{\partial^2\breve{\phi}}{\partial\zeta^2} + Le\Pr\breve{f}\frac{\partial\breve{\phi}}{\partial\zeta} + \frac{N_t}{N_b}\frac{\partial^2\breve{\theta}}{\partial\zeta^2}. \tag{24}$$

Here þ ∈[0,1] represents the embedding parameter, $\hbar_f$, $\hbar_\theta$ and $\hbar_\phi$ the non-zero auxiliary parameters and $\mathbf{N}_f$, $\mathbf{N}_\theta$ and $\mathbf{N}\phi$ the nonlinear operators. For þ = 0 and þ = 1 we have

$$\breve{f}(\zeta;0) = f_0(\zeta), \ \breve{f}(\zeta;1) = f(\zeta), \tag{25}$$

$$\breve{\theta}(\zeta,0) = \theta_0(\zeta), \ \breve{\theta}(\zeta,1) = \theta(\zeta), \tag{26}$$

$$\breve{\phi}(\zeta,0) = \phi_0(\zeta), \ \breve{\phi}(\zeta,1) = \phi(\zeta). \tag{27}$$

When þ changes from 0 to 1 then $\breve{f}(\zeta;\text{þ})$, $\breve{\theta}(\zeta,\text{þ})$ and $\breve{\phi}(\zeta,\text{þ})$ vary from primary approximations $f_0(\zeta)$, $\theta_0(\zeta)$ and $\phi_0(\zeta)$ to the desired solutions $f(\zeta)$, $\theta(\zeta)$ and $\phi(\zeta)$. The following expressions by Taylor's series expansion can be written as

$$\breve{f}(\zeta;\ \text{þ}) = f_0(\zeta) + \sum_{\hat{m}=1}^{\infty} f_{\hat{m}}(\zeta)\text{þ}^{\hat{m}},\ f_{\hat{m}}(\zeta) = \frac{1}{\hat{m}!}\frac{\partial^{\hat{m}}\breve{f}(\zeta,\ \text{þ})}{\partial \text{þ}^{\hat{m}}}\bigg|_{\text{þ}=0}, \tag{28}$$

$$\breve{\theta}(\zeta,\ \text{þ}) = \theta_0(\zeta) + \sum_{\hat{m}=1}^{\infty} \theta_{\hat{m}}(\zeta)\text{þ}^{\hat{m}},\ \theta_{\hat{m}}(\zeta) = \frac{1}{\hat{m}!}\frac{\partial^{\hat{m}}\breve{\theta}(\zeta,\ \text{þ})}{\partial \text{þ}^{\hat{m}}}\bigg|_{\text{þ}=0}, \tag{29}$$

$$\breve{\phi}(\zeta,\ \text{þ}) = \phi_0(\zeta) + \sum_{\hat{m}=1}^{\infty} \phi_{\hat{m}}(\zeta)\text{þ}^{\hat{m}},\ \phi_{\hat{m}}(\zeta) = \frac{1}{\hat{m}!}\frac{\partial^{\hat{m}}\breve{\phi}(\zeta,\ \text{þ})}{\partial \text{þ}^{\hat{m}}}\bigg|_{\text{þ}=0}. \tag{30}$$

The convergence of above series expressions strongly depends upon $\hbar_f$, $\hbar_\theta$ and $\hbar_\phi$. The values of $\hbar_f$, $\hbar_\theta$ and $\hbar_\phi$ are chosen so that Eqs (28)–(30) converge at þ = 1 then

$$f(\zeta) = f_0(\zeta) + \sum_{\hat{m}=1}^{\infty} f_{\hat{m}}(\zeta), \tag{31}$$

$$\theta(\zeta) = \theta_0(\zeta) + \sum_{\hat{m}=1}^{\infty} \theta_{\hat{m}}(\zeta), \tag{32}$$

$$\phi(\zeta) = \phi_0(\zeta) + \sum_{\hat{m}=1}^{\infty} \phi_{\hat{m}}(\zeta). \tag{33}$$

The $\hat{m}$ th-order deformation problems can be expressed as follows:

$$\mathbf{L}_f[f_{\hat{m}}(\zeta) - \chi_{\hat{m}} f_{\hat{m}-1}(\zeta)] = \hbar_f \widetilde{\mathbf{R}}_f^{\hat{m}}(\zeta), \tag{34}$$

$$\mathbf{L}_\theta[\theta_{\hat{m}}(\zeta) - \chi_{\hat{m}} \theta_{\hat{m}-1}(\zeta)] = \hbar_\theta \widetilde{\mathbf{R}}_\theta^{\hat{m}}(\zeta), \tag{35}$$

$$\mathbf{L}_\phi[\phi_{\hat{m}}(\zeta) - \chi_{\hat{m}} \phi_{\hat{m}-1}(\zeta)] = \hbar_\phi \widetilde{\mathbf{R}}_\phi^{\hat{m}}(\zeta), \tag{36}$$

$$\left.\begin{aligned} f_{\hat{m}}(0) = f'_{\hat{m}}(0) = f'_{\hat{m}}(\infty) = 0,\ \theta'_{\hat{m}}(0) - \gamma\theta_{\hat{m}}(0) = 0, \\ Nb\phi'_{\hat{m}}(0) + Nt\theta'_{\hat{m}}(0) = 0,\ \theta_{\hat{m}}(\infty) = \phi_{\hat{m}}(\infty) = 0, \end{aligned}\right\} \tag{37}$$

$$\begin{aligned} \widetilde{\mathbf{R}}_f^{\hat{m}}(\zeta) = f'''_{\hat{m}-1} + \beta_1 \sum_{k=0}^{\hat{m}-1}\left(\left(\frac{3n-1}{2}\right) f''_{\hat{m}-1-k} f''_k - \left(\frac{n+1}{2}\right) f_{\hat{m}-1-k} f''''_k + (n-1) f_{\hat{m}-1-k} f'''_k\right) \\ +(1+\lambda_1)\sum_{k=0}^{\hat{m}-1}\left(f_{\hat{m}-1-k} f''_k - \left(\frac{2n}{n+1}\right) f'_{\hat{m}-1-k} f'_k\right) - (1+\lambda_1)\left(\frac{2}{n+1}\right)(Ha)^2 f'_{\hat{m}-1}, \end{aligned} \tag{38}$$

$$\widetilde{\mathbf{R}}_{\theta}^{\hat{m}}(\zeta)=\frac{1}{\Pr}\theta_{\hat{m}-1}''+\sum_{k=0}^{\hat{m}-1}f_{\hat{m}-1-k}\theta_{k}'+N_{b}\sum_{k=0}^{\hat{m}-1}\theta_{\hat{m}-1-k}'\phi_{k}' +N_{t}\sum_{k=0}^{\hat{m}-1}\theta_{\hat{m}-1-k}'\theta_{k}'+\left(\frac{2}{n+1}\right)S_{1}\theta_{\hat{m}-1}, \tag{39}$$

$$\widetilde{\mathbf{R}}_{\phi}^{\hat{m}}(\zeta)=\phi_{\hat{m}-1}''+Le\Pr\sum_{k=0}^{\hat{m}-1}(f_{\hat{m}-1-k}\phi_{k}')+\frac{N_{t}}{N_{b}}\theta_{\hat{m}-1}'', \tag{40}$$

$$\boldsymbol{\chi}_{\hat{m}}=\begin{cases}0, & \hat{m}\leq 1,\\ 1, & \hat{m}>1.\end{cases} \tag{41}$$

General expressions of $(f_{\hat{m}},\theta_{\hat{m}},\phi_{\hat{m}})$ through special solutions $(f_{\hat{m}}^{*},\ \theta_{\hat{m}}^{*},\ \phi_{\hat{m}}^{*})$ are presented by the following expressions:

$$f_{\hat{m}}(\zeta)=f_{\hat{m}}^{*}(\zeta)+B_{1}^{*}+B_{2}^{*}e^{\zeta}+B_{3}^{*}e^{-\zeta}, \tag{42}$$

$$\theta_{\hat{m}}(\zeta)=\theta_{\hat{m}}^{*}(\zeta)+B_{4}^{*}e^{\zeta}+B_{5}^{*}e^{-\zeta}, \tag{43}$$

$$\phi_{\hat{m}}(\zeta)=\phi_{\hat{m}}^{*}(\zeta)+B_{6}^{*}e^{\zeta}+B_{7}^{*}e^{-\zeta}, \tag{44}$$

in which the constants B_{j}^{*} $(j=1\text{–}7)$ through the boundary condition (37) are given by

$$B_{2}^{*}=B_{4}^{*}=B_{6}^{*}=0,\ B_{3}^{*}=\left.\frac{\partial f_{\hat{m}}^{*}(\zeta)}{\partial\zeta}\right|_{\zeta=0},\ B_{1}^{*}=-B_{3}^{*}-f_{\hat{m}}^{*}(0), \tag{45}$$

$$B_{5}^{*}=\frac{1}{1+\gamma}\left(\left.\frac{\partial\theta_{\hat{m}}^{*}(\zeta)}{\partial\zeta}\right|_{\zeta=0}-\gamma\theta_{\hat{m}}^{*}(0)\right), \tag{46}$$

$$B_{7}^{*}=\left.\frac{\partial\phi_{\hat{m}}^{*}(\zeta)}{\partial\zeta}\right|_{\zeta=0}+\frac{N_{t}}{N_{b}}\left(-B_{5}^{*}+\left.\frac{\partial\theta_{\hat{m}}^{*}(\zeta)}{\partial\zeta}\right|_{\zeta=0}\right). \tag{47}$$

4. Convergence analysis

The expressions (31)–(33) contain $\hbar_{f}$, $\hbar_{\theta}$ and $\hbar_{\phi}$. Obviously the convergence is accelerated by the auxiliary parameters $\hbar_{f}$, $\hbar_{\theta}$ and $\hbar_{\phi}$ for the series solutions. For appropriate values of $\hbar_{f}$, $\hbar_{\theta}$ and $\hbar_{\phi}$, the $\hbar-$ curves at 15th order of approximations are sketched. It is apparent from Fig 1 that the admissible ranges of $\hbar_{f}$, $\hbar_{\theta}$ and $\hbar_{\phi}$ are $-1.35\leq\hbar_{f}\leq-0.15$, $-1.50\leq\hbar_{\theta}\leq-0.15$ and $-1.60\leq\hbar_{\phi}\leq-0.15$ respectively. The residual errors for velocity, temperature and

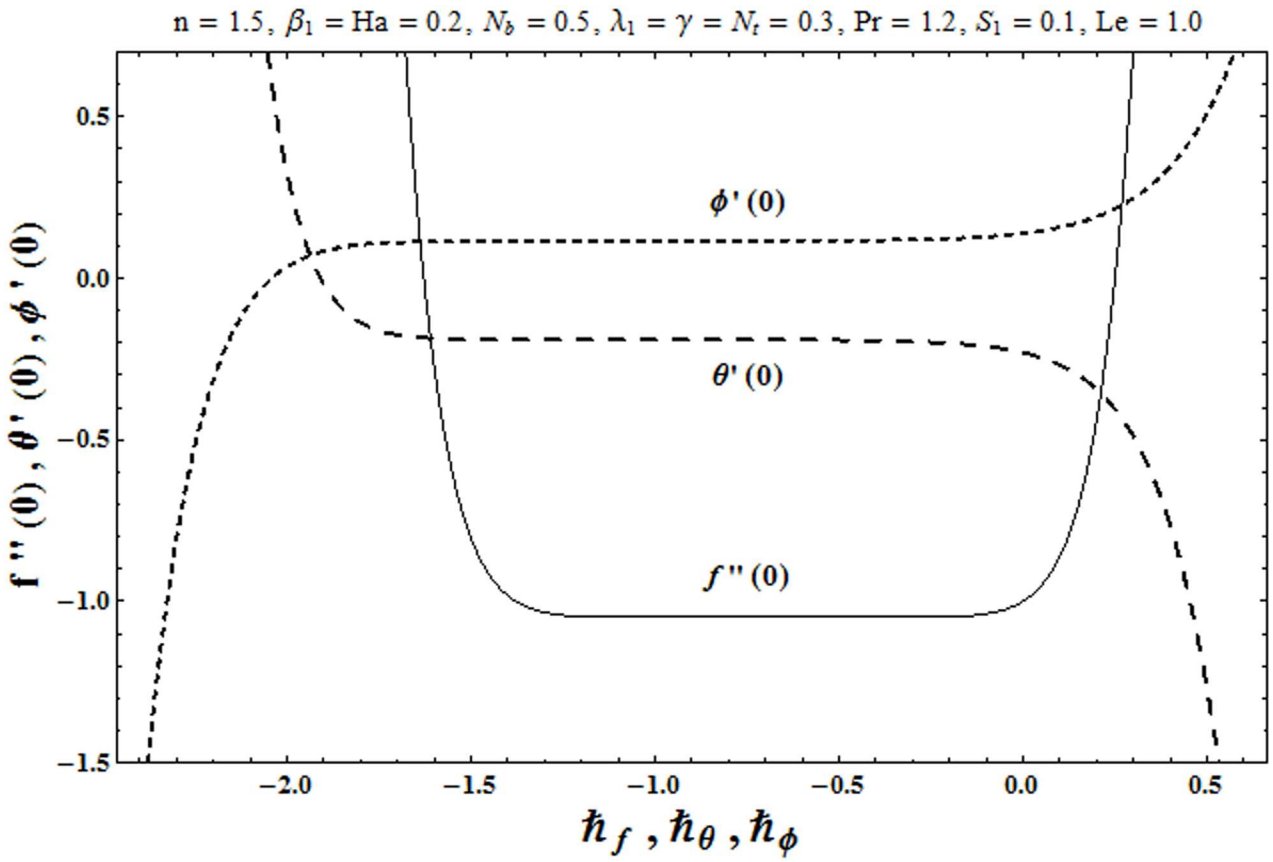

Fig 1. The $\hbar$ – curves for *f*, θ and ϕ.

doi:10.1371/journal.pone.0172518.g001

concentration distributions are calculated through the following expressions:

$$\Delta_m^f = \int_0^1 [\widetilde{\mathbf{R}}_{\dot{m}}^f(\zeta, \hbar_f)]^2 d\zeta, \tag{48}$$

$$\Delta_m^\theta = \int_0^1 [\widetilde{\mathbf{R}}_{\dot{m}}^\theta(\zeta, \hbar_\theta)]^2 d\zeta, \tag{49}$$

$$\Delta_m^\phi = \int_0^1 [\widetilde{\mathbf{R}}_{\dot{m}}^\phi(\zeta, \hbar_\phi)]^2 d\zeta. \tag{50}$$

To get the suitable range for $\hbar$, the $\hbar$– curves for the residual errors of velocity, temperature and concentration distributions are plotted in the Figs 2–4. It is observed that the correct results up to fifth decimal place are obtained for values of $\hbar$ from this range. Table 1 presents that the 24th order of deformations is enough for the convergent series solutions of velocity, temperature and concentration distributions.

5. Discussion

This portion organized the impacts of local Deborah number β_1, Hartman number *Ha*, Brownian motion parameter N_b, ratio of relaxation to retardation times λ_1, Biot number γ,

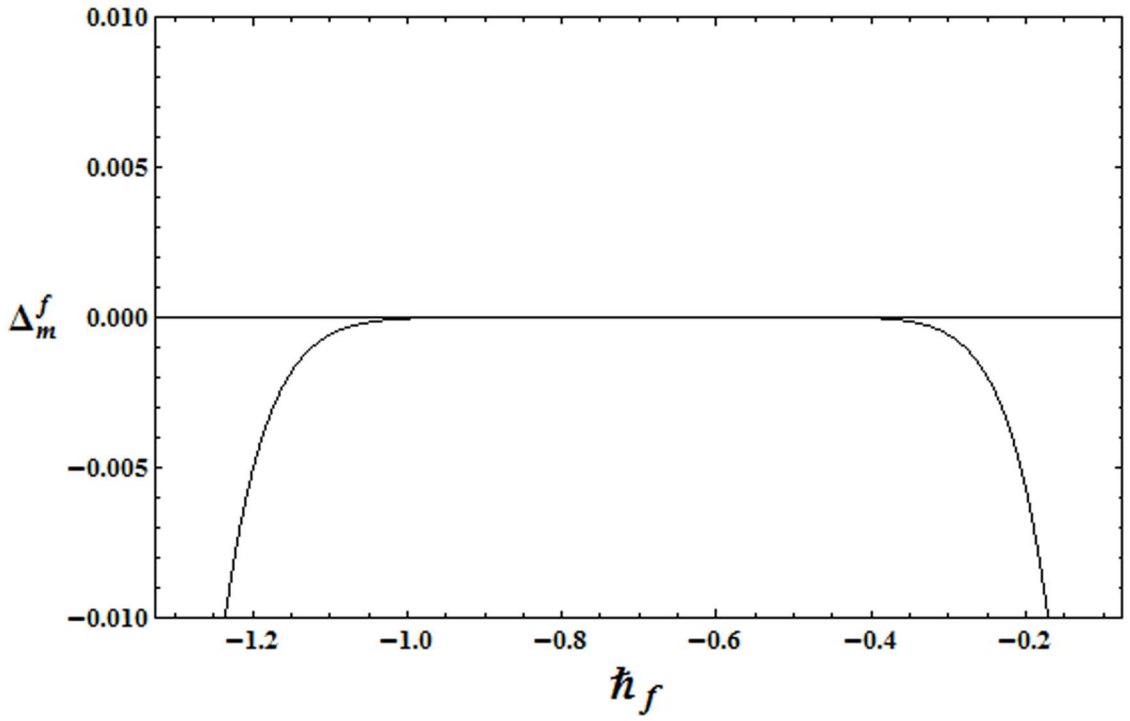

Fig 2. $\hbar_f$ **– curve for the residual error** Δ_m^f**.**

doi:10.1371/journal.pone.0172518.g002

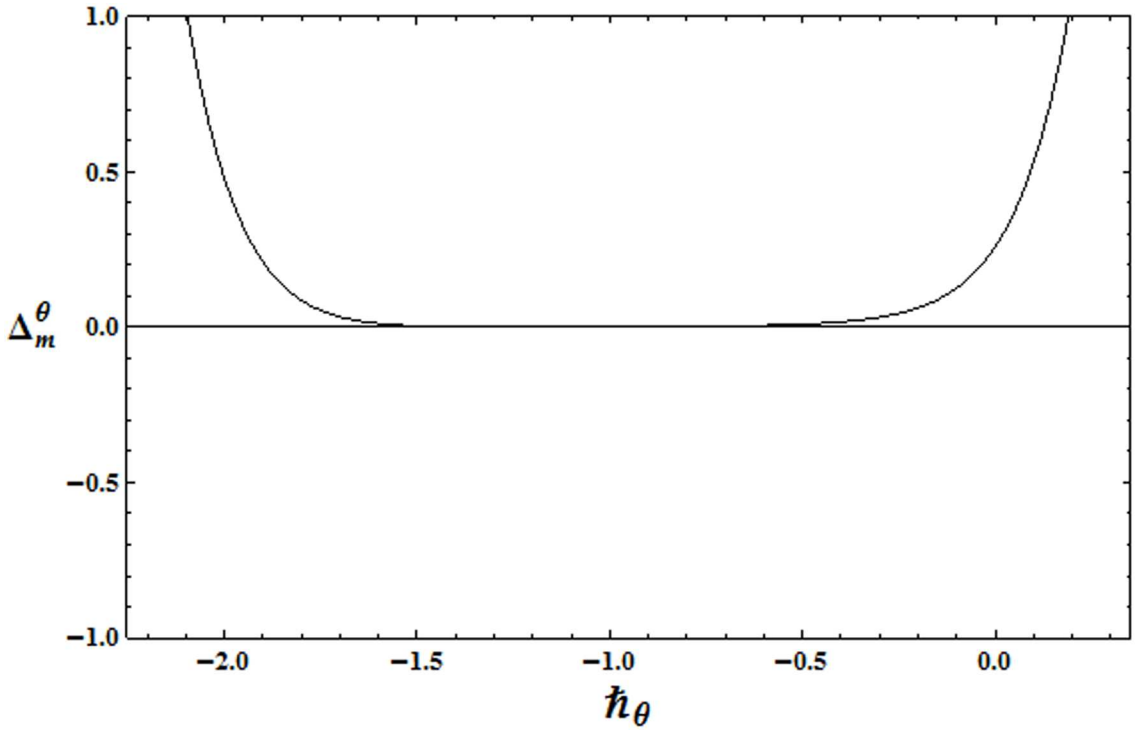

Fig 3. $\hbar_f$ **– curve for the residual error** Δ_m^θ**.**

doi:10.1371/journal.pone.0172518.g003

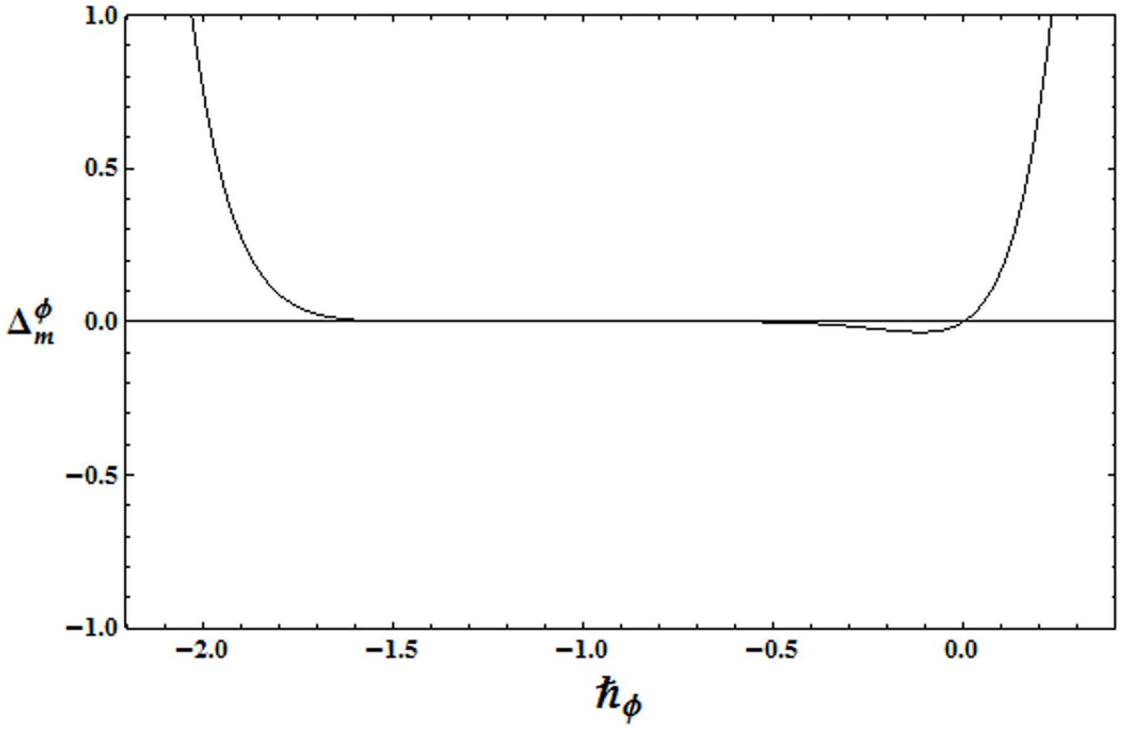

Fig 4. $\hbar_{\phi}$ **– curve for the residual error** Δ_m^{ϕ}.

doi:10.1371/journal.pone.0172518.g004

thermophoresis parameter N_t, Prandtl number Pr, heat generation/absorption parameter S_1 and Lewis number Le on the temperature $\theta(\zeta)$ and concentration $\phi(\zeta)$. Fig 5 illustrates that how local Deborah number β_1 affects the temperature distribution $\theta(\zeta)$. It is analyzed that temperature $\theta(\zeta)$ and related thermal layer thickness are decreased for larger local Deborah number β_1. Physically there exists a direct relationship between local Deborah number β_1 and retardation time. Hence by increasing local Deborah number β_1, the retardation time is also enhanced. Such enhancement in retardation time corresponds to lower temperature distribution $\theta(\zeta)$ and thinner thermal layer thickness. Influence of λ_1 on temperature distribution $\theta(\zeta)$ is shown in Fig 6. For larger λ_1, the relaxation time increases and retardation time decays. Thus temperature distribution $\theta(\zeta)$ and thermal layer thickness are increased. Fig 7 presents variation in temperature distribution $\theta(\zeta)$ for Hartman number Ha. An increase in Hartman number corresponds to more temperature $\theta(\zeta)$ and thermal layer thickness. As expected the

Table 1. Homotopic solutions convergence when $n = 1.5$, $\beta_1 = Ha = 0.2$, $N_b = 0.5$, $\lambda_1 = \gamma = N_t = 0.3$, Pr = 1.2, S1 = 0.1, and $Le = 1.0$.

Order of approximations	$-f''(0)$	$-\theta'(0)$	$-\phi'(0)$
1	1.05680	0.21543	0.12926
8	1.04981	0.19237	0.11542
15	1.04981	0.19085	0.11451
24	1.04981	0.19065	0.11439
30	1.04981	0.19065	0.11439
40	1.04981	0.19065	0.11439
50	1.04981	0.19065	0.11439

doi:10.1371/journal.pone.0172518.t001

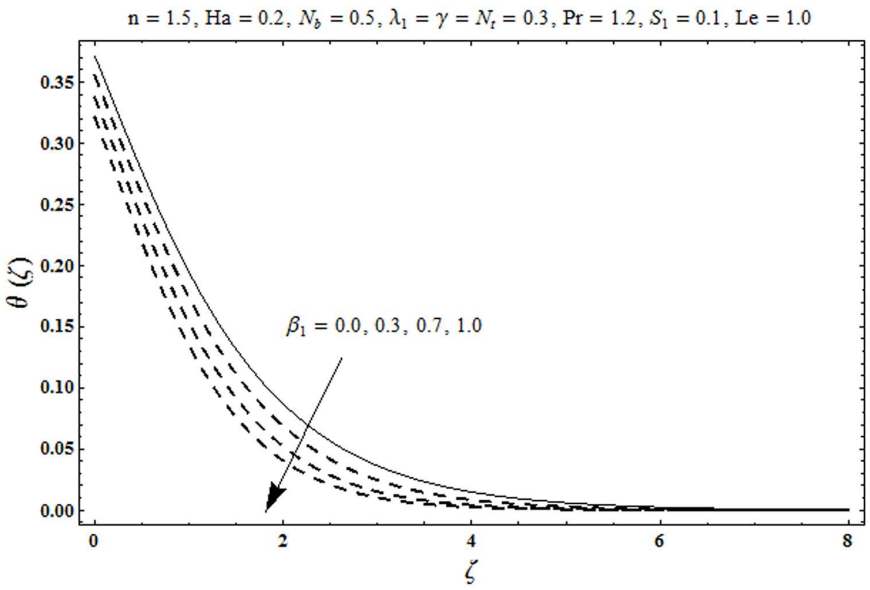

Fig 5. Plots of temperature $\theta(\zeta)$ for local Deborah number β_1.

doi:10.1371/journal.pone.0172518.g005

magnetic field introduces the retarding body force that acts transverse to the direction of an applied magnetic field. It retards the fluid motion and as a result the temperature distribution $\theta(\zeta)$ enhances. This body force is known as Lorentz force. Fig 8 presents the impact of Biot number γ on temperature $\theta(\zeta)$. Stronger convection is caused by increasing Biot number γ. Therefore the temperature $\theta(\zeta)$ and thermal layer thickness are enhanced. Variation in temperature $\theta(\zeta)$ due to heat generation/absorption parameter S_1 is shown in Fig 9. Here $S_1 > 0$ represents heat generation and $S_1 < 0$ yields heat absorption. Temperature profile and related

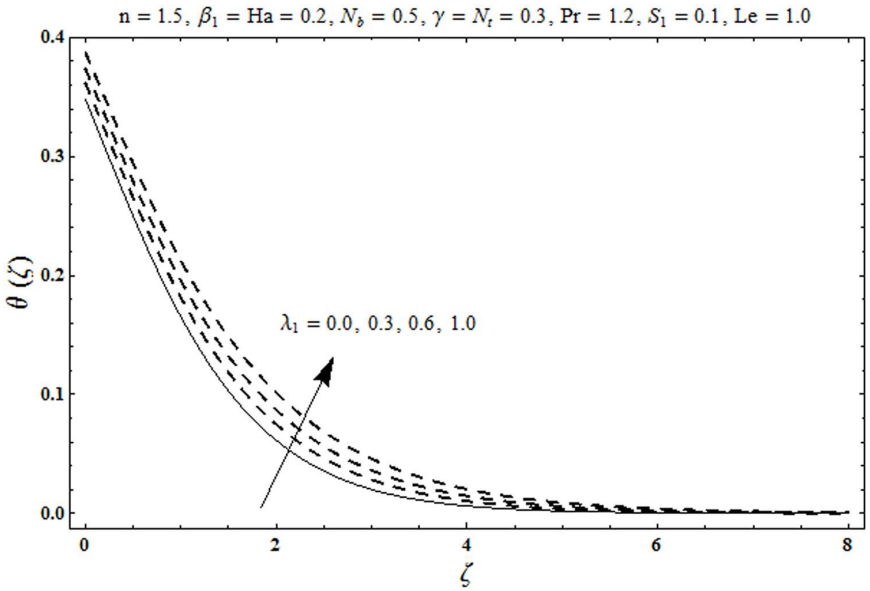

Fig 6. Plots of temperature profile $\theta(\zeta)$ for ratio of relaxation to retardation time λ_1.

doi:10.1371/journal.pone.0172518.g006

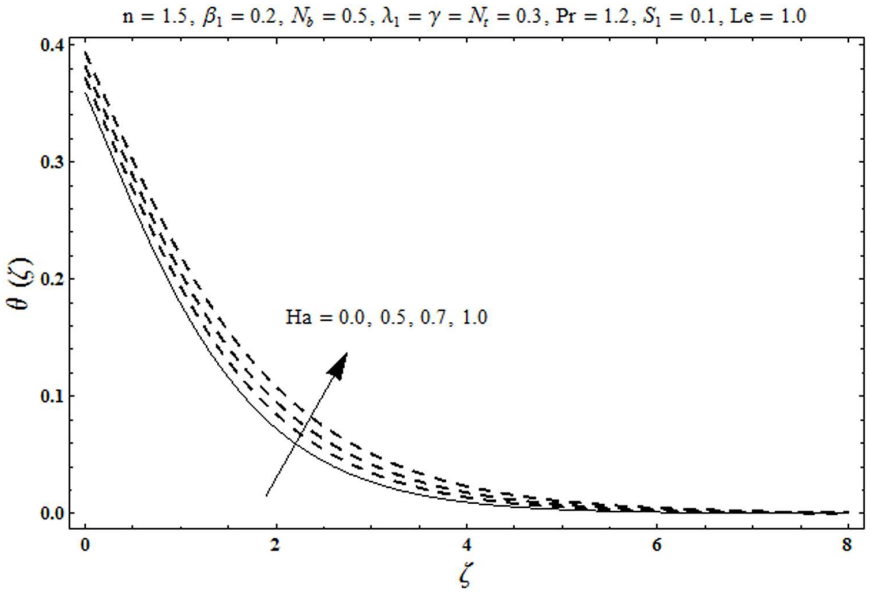

Fig 7. Plots of temperature profile *θ(ζ)* for Hartman number *Ha*.

doi:10.1371/journal.pone.0172518.g007

thermal layer thickness have increasing behavior for heat generation but it is not the case for heat absorption. Fig 10 demonstrates the variation of temperature $\theta(\zeta)$ for Prandtl number Pr. It is observed that temperature $\theta(\zeta)$ and thermal layer thickness are decreasing functions of Pr. Physically Prandtl number Pr is an integral part of thermal diffusivity. Thermal diffusivity is responsible for lower temperature $\theta(\zeta)$ and thermal layer thickness. Higher values of Prandtl number yields weaker thermal diffusivity which corresponds to lower temperature and less thickness of thermal layer. Fig 11 is drawn for impact of thermophoresis parameter N_t on temperature $\theta(\zeta)$. Larger thermophoresis parameter N_t lead to higher temperature and more

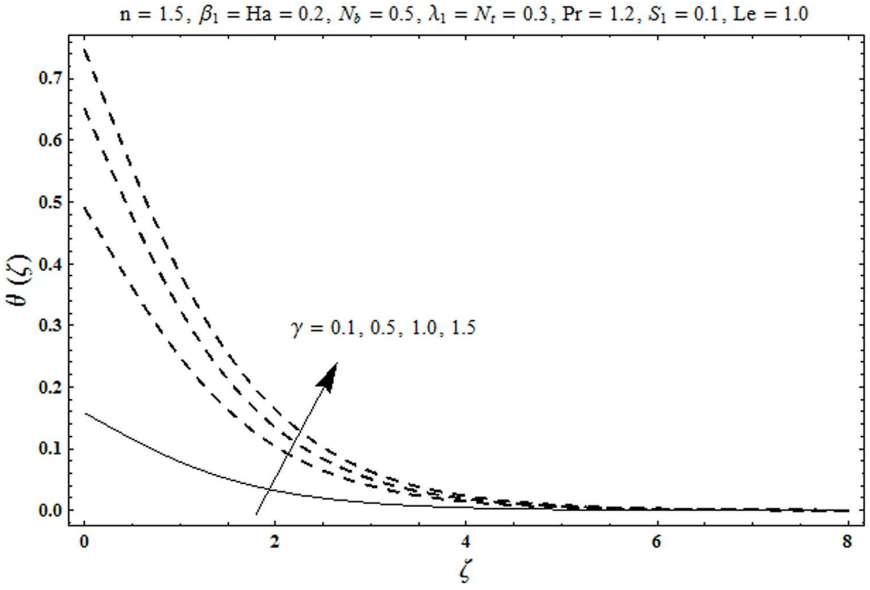

Fig 8. Plots of temperature profile *θ(ζ)* for Biot number *γ*.

doi:10.1371/journal.pone.0172518.g008

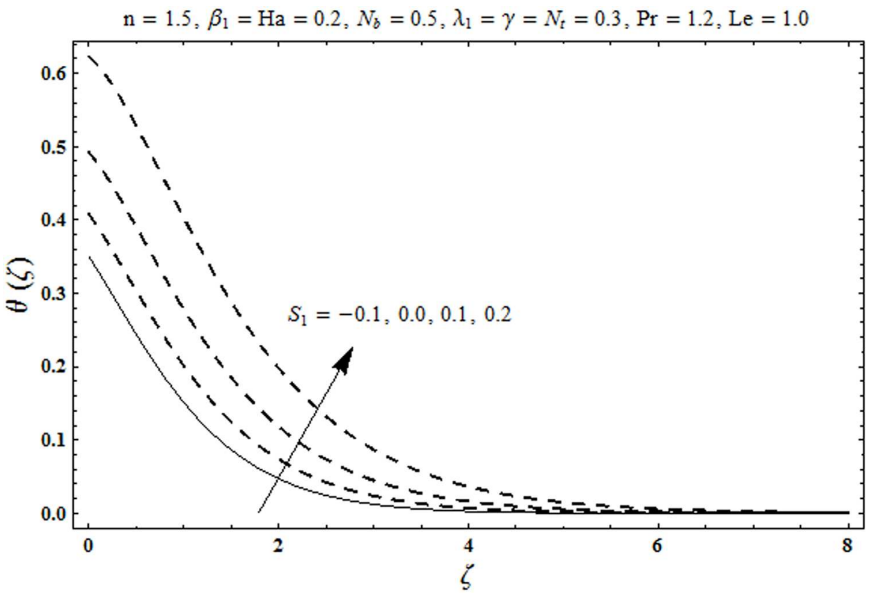

Fig 9. Plots of temperature profile *θ(ζ)* for heat generation/absorption parameter S_1.

doi:10.1371/journal.pone.0172518.g009

thermal layer thickness. Actually an enhancement in N_t yields a stronger thermophoretic force which allows deeper migration of nanoparticles in the fluid. Far away from the surface there is higher temperature field and more thickness of thermal layer. Fig 12 is sketched to examine concentration field $\phi(\zeta)$ for local Deborah number β_1. Here concentration field is weaker for larger values of β_1. Concentration field $\phi(\zeta)$ enhances when λ_1 increases (see Fig 13). Fig 14

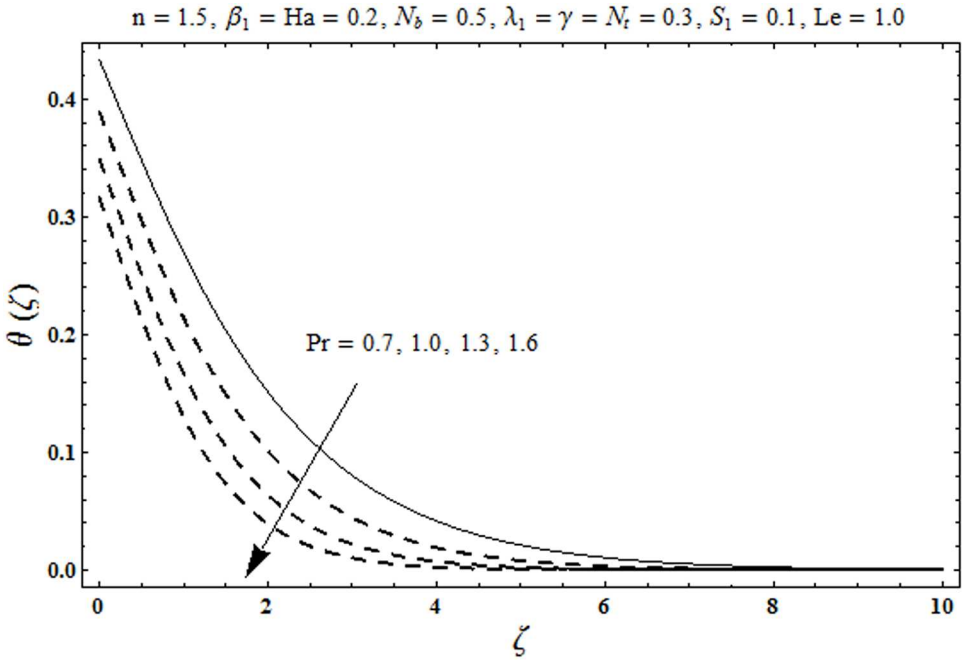

Fig 10. Plots of temperature profile *θ(ζ)* for Prandtk number Pr.

doi:10.1371/journal.pone.0172518.g010

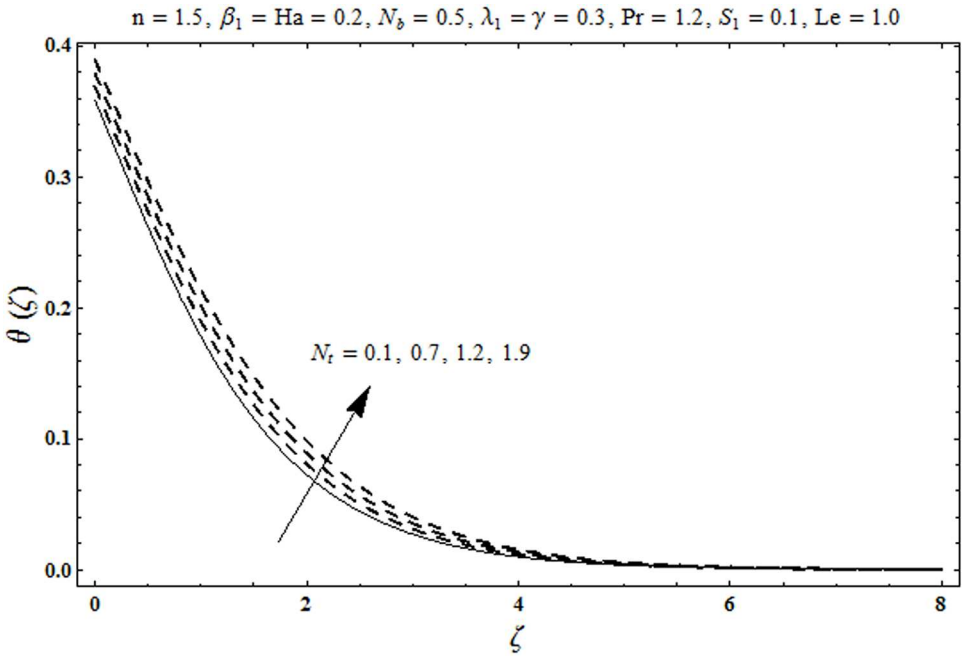

Fig 11. Plots of temperature profile $\theta(\zeta)$ for thermophoresis parameter N_t.

doi:10.1371/journal.pone.0172518.g011

shows impact of Hartman number *Ha* on concentration $\phi(\zeta)$. The concentration $\phi(\zeta)$ and associated layer thickness are enhanced for larger Hartman number. From Fig 15 we observed that an increase in Biot number γ yields an enhancement in concentration profile $\phi(\zeta)$ and its related boundary layer thickness. Larger Lewis number *Le* indicate decay in the concentration

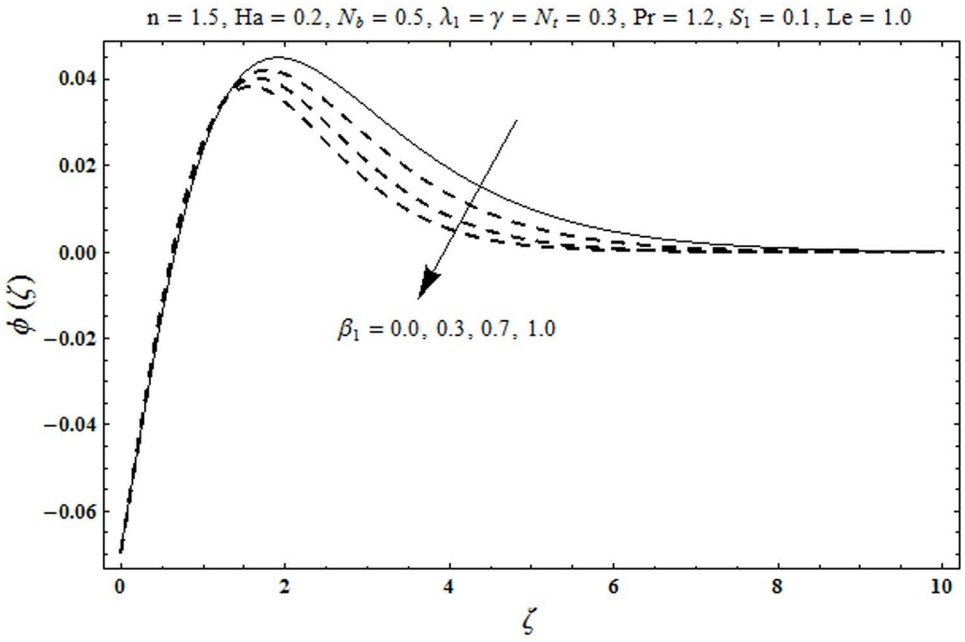

Fig 12. Plots of concentration profile $\phi(\zeta)$ for local Deborah number β_1.

doi:10.1371/journal.pone.0172518.g012

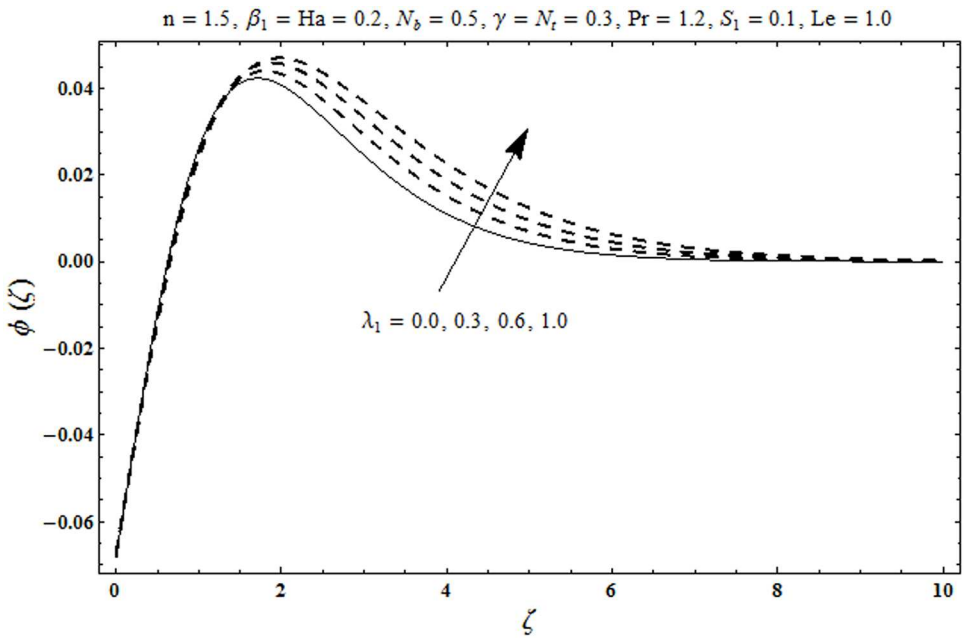

Fig 13. Plots of concentration profile $\phi(\zeta)$ for ratio of relaxation to retardation time λ_1.

doi:10.1371/journal.pone.0172518.g013

field $\phi(\zeta)$ (see Fig 16). Physically Lewis number is based on Brownian diffusivity. An increase in Lewis number *Le* yields weaker Brownian diffusivity. Such weaker Brownian diffusivity corresponds to lower concentration field $\phi(\zeta)$. Fig 17 addresses variation of Prandtl number Pr on concentration $\phi(\zeta)$. The concentration $\phi(\zeta)$ and associated thickness of boundary layer are decreased for higher Prandtl number Pr. From Fig 18 it is clearly examined that a weaker

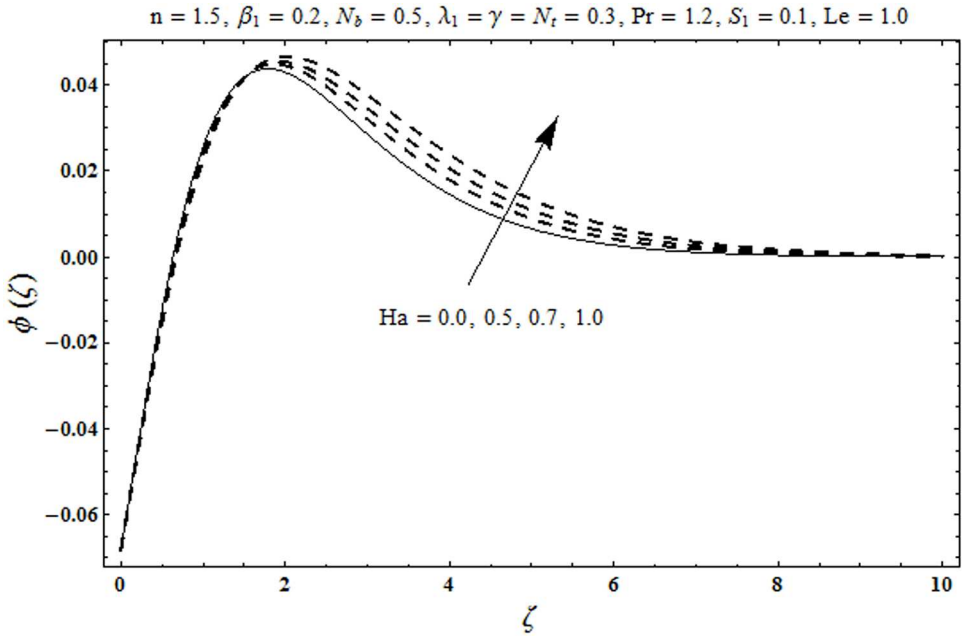

Fig 14. Plots of concentration profile $\phi(\zeta)$ for Hartman number *Ha*.

doi:10.1371/journal.pone.0172518.g014

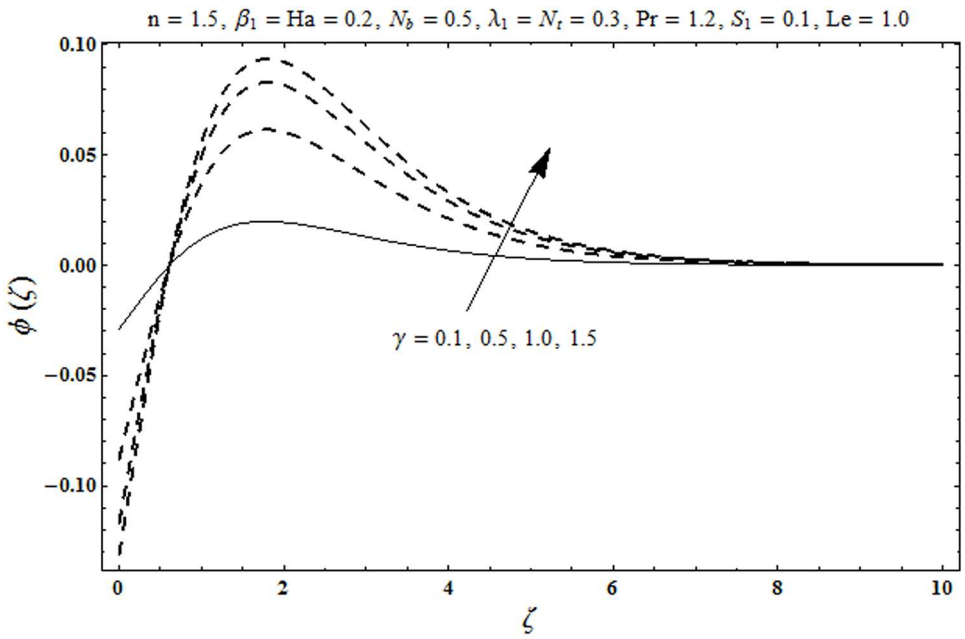

Fig 15. Plots of concentration profile $\phi(\zeta)$ for Boit number γ.

doi:10.1371/journal.pone.0172518.g015

concentration profile $\phi(\zeta)$ is generated by higher Brownian motion parameter N_b. Fig 19 shows that the larger thermophoresis parameter N_t yields a higher concentration profile $\phi(\zeta)$. Table 2 is calculated for numerical computations of local Nusselt number $Re_x^{-1/2}Nu_x$ via β_1, λ_1, Ha, γ, S_1, N_t, N_b, Le and Pr when $n = 1.5$. Here we noticed that the local Nusselt number has

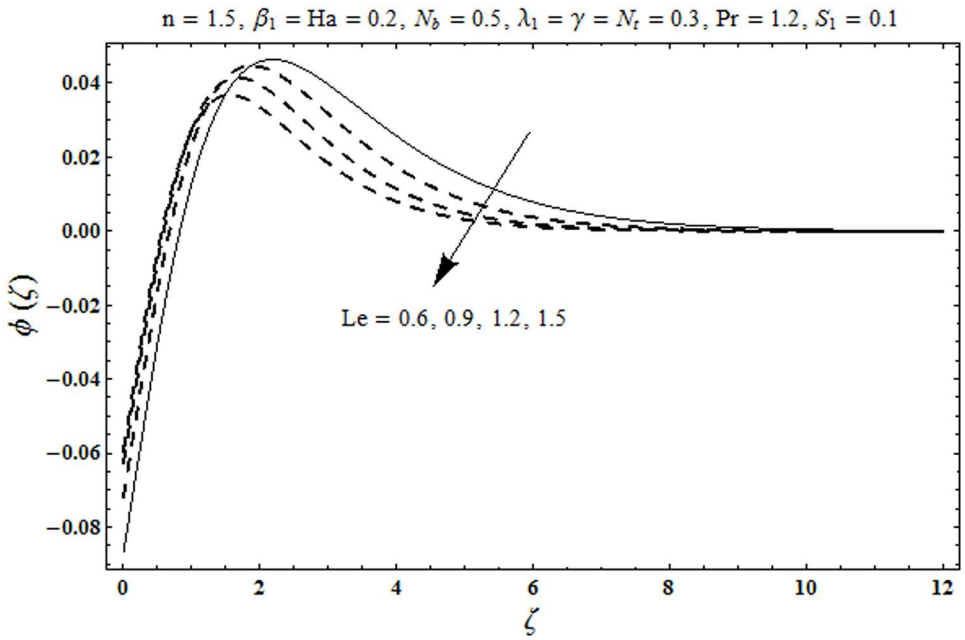

Fig 16. Plots of concentration profile $\phi(\zeta)$ for Lewis number *Le*.

doi:10.1371/journal.pone.0172518.g016

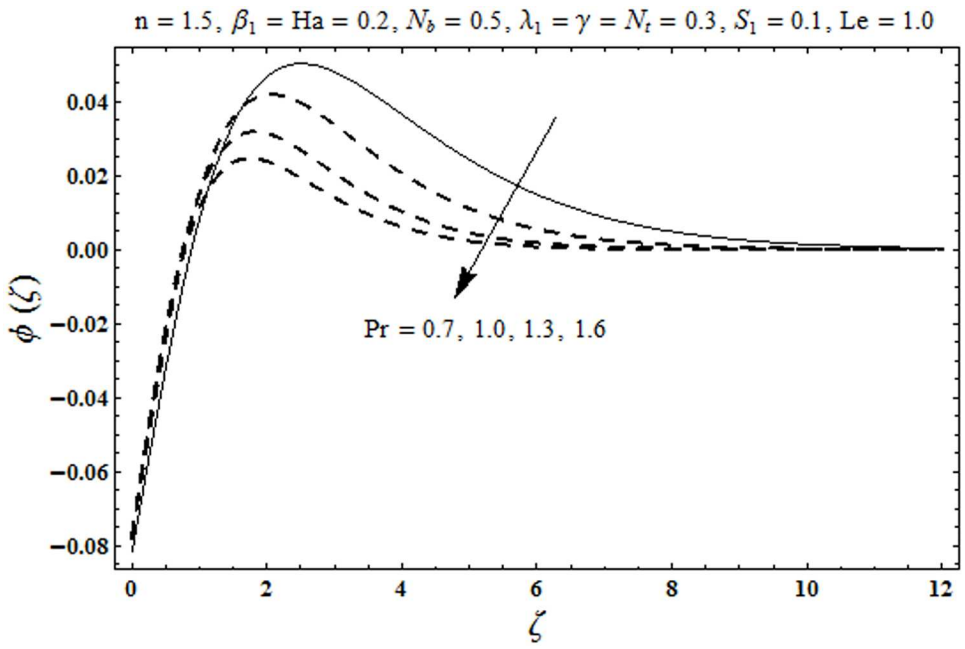

Fig 17. Plots of concentration profile $\phi(\zeta)$ for Prandtl number Pr.

doi:10.1371/journal.pone.0172518.g017

higher values for larger Prandtl number Pr while opposite trend is noticed for Lewis number *Le*. It is also observed that λ_1, S_1 and *Ha* yield lower local Nusselt number. The local Deborah number β_1 shows opposite behavior for local Nusselt number when compared with aforementioned parameters.

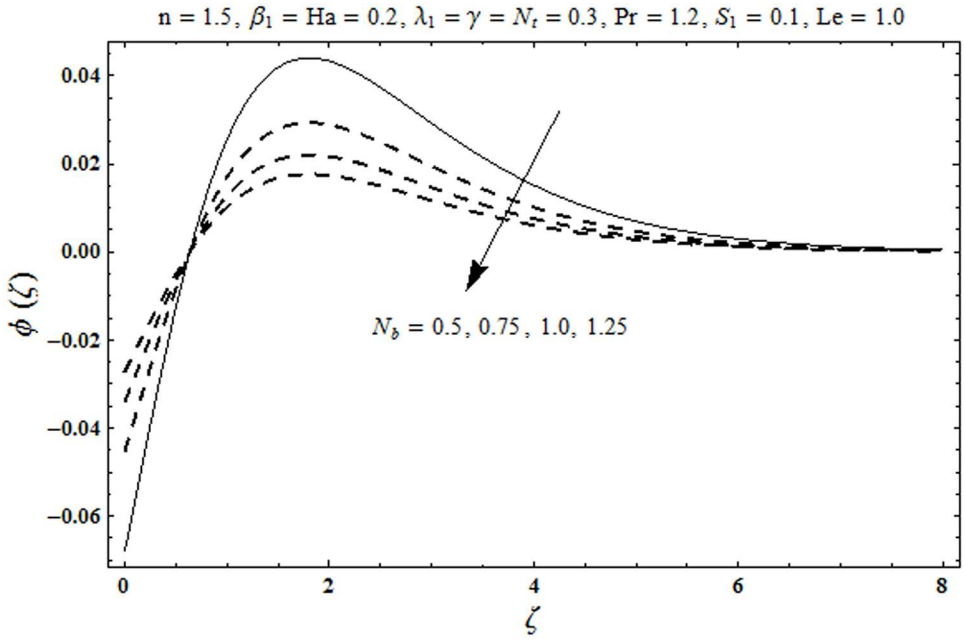

Fig 18. Plots of concentration profile $\phi(\zeta)$ for Brownian motion parameter N_b.

doi:10.1371/journal.pone.0172518.g018

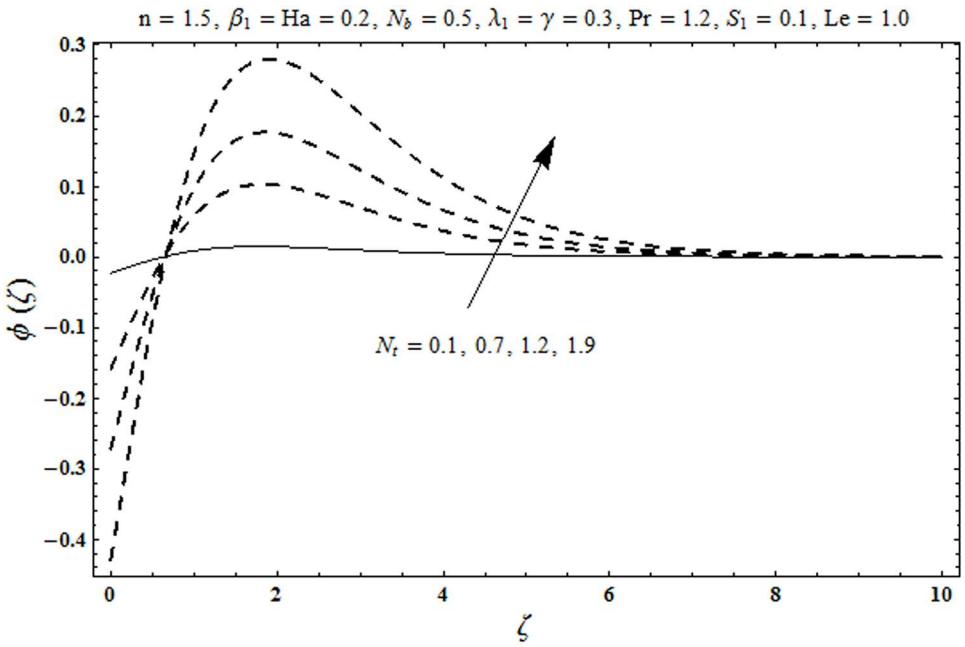

Fig 19. Plots of concentration profile $\phi(\zeta)$ for thermophoresis motion parameter N_t.

doi:10.1371/journal.pone.0172518.g019

Table 2. Numerical calculations of local Nusselt number $Re_x^{-1/2}Nu_x$ for different values of $\beta 1$, λ_1, Ha, γ, S_1, N_t, N_b, Le and Pr when $n = 1.5$.

β_1	λ_1	Ha	γ	S_1	N_t	N_b	Le	Pr	$Re_x^{-1/2}Nu_x$
0.0	0.3	0.2	0.3	0.1	0.3	0.5	1.0	1.2	0.2060
0.3									0.2158
0.6									0.2210
0.2	0.0	0.2	0.3	0.1	0.3	0.5	1.0	1.2	0.2187
	0.5								0.2098
	1.0								0.2004
0.2	0.3	0.2	0.3	0.1	0.3	0.5	1.0	1.2	0.2133
		0.5							0.2088
		0.8							0.2003
0.2	0.3	0.2	0.1	0.1	0.3	0.5	1.0	1.2	0.0941
			0.6						0.3107
			1.2						0.4007
0.2	0.3	0.2	0.3	0.0	0.3	0.5	1.0	1.2	0.2282
				0.1					0.2133
				0.2					0.1839
0.2	0.3	0.2	0.3	0.1	0.0	0.5	1.0	1.2	0.2151
					0.5				0.2119
					1.0				0.2082
0.2	0.3	0.2	0.3	0.1	0.3	0.5		1.2	0.2133
						1.0	1.0		0.2133
						1.5			0.2133
0.2	0.3	0.2	0.3	0.1	0.3	0.5	0.5	1.2	0.2140
							1.0		0.2133
							1.5		0.2128
0.2	0.3	0.2	0.3	0.1	0.3	0.5	1.0	1.0	0.2017
								1.5	0.2260
								2.0	0.2403

doi:10.1371/journal.pone.0172518.t002

6. Conclusions

Magnetohydrodynamic (MHD) flow of Jeffrey nanofluid bounded by a nonlinear stretching surface with heat generation/absorption is investigated. The observations are summarized in the following points.

- An increase in local Deborah number β_1 depicts a decreasing behavior for temperature $\theta(\zeta)$ and concentration $\phi(\zeta)$ profiles.
- Both temperature $\theta(\zeta)$ and concentration $\phi(\zeta)$ profiles are enhanced when ratio of relaxation to retardation times λ_1 is increased.
- An increase in Hartman number *Ha* shows higher temperature $\theta(\zeta)$ and concentration $\phi(\zeta)$ profiles.
- Biot number γ has similar effects for temperature $\theta(\zeta)$ and concentration $\phi(\zeta)$ profiles.
- Prandtl number Pr indicates qualitatively similar behavior for both temperature $\theta(\zeta)$ and concentration $\phi(\zeta)$ profiles.
- Temperature profile $\theta(\zeta)$ and associated thermal layer thickness are increasing functions of heat generation/absorption parameter S_1.
- Concentration profile $\phi(\zeta)$ decays for larger Brownian motion parameter N_b.
- Increasing behavior is noted for temperature $\theta(\zeta)$ and concentration $\phi(\zeta)$ profiles for larger thermophoresis parameter N_t.
- Local Nusselt number reduces for larger N_t but it remains constant for N_b.

Author Contributions

Conceptualization: TH A. Aziz TM A. Alsaedi.

Data curation: TH A. Aziz TM A. Alsaedi.

Formal analysis: TH A. Aziz TM A. Alsaedi.

Investigation: TH A. Aziz TM A. Alsaedi.

Methodology: TH A. Aziz TM A. Alsaedi.

Project administration: TH A. Aziz TM A. Alsaedi.

Resources: TH A. Aziz TM A. Alsaedi.

Software: TH A. Aziz TM A. Alsaedi.

Supervision: TH A. Aziz TM A. Alsaedi.

Validation: TH A. Aziz TM A. Alsaedi.

Visualization: TH A. Aziz TM A. Alsaedi.

Writing – original draft: TH A. Aziz TM A. Alsaedi.

Writing – review & editing: TH A. Aziz TM A. Alsaedi.

References

1. Choi SUS, Eastman JA. Enhancing thermal conductivity of fluids with nanoparticles. ASME International Mechanical Engineering Congress & Exposition, American Society of Mechanical Engineers, San Francisco 1995.
2. Buongiorno J. Convective transport in nanofluids. ASME J Heat Transfer. 2006; 128: 240–250.
3. Khan WA, Pop I. Boundary-layer flow of a nanofluid past a stretching sheet. Int J Heat Mass Transfer. 2010; 53: 2477–2483.
4. Turkyilmazoglu M, Pop I. Heat and mass transfer of unsteady natural convection flow of some nanofluids past a vertical infinite flat plate with radiation effect. Int J Heat Mass Transfer. 2013; 59: 167–171.
5. Ibrahim W, Makinde OD. The effect of double stratification on boundary-layer flow and heat transfer of nanofluid over a vertical plate. Comput Fluids. 2013; 86: 433–441.
6. Sheikholeslami M, Hatami M, Ganji DD. Nanofluid flow and heat transfer in a rotating system in the presence of a magnetic field. J Mol Liq. 2014; 190: 112–120.
7. Zeeshan A, Baig M, Ellahi R, Hayat T. Flow of viscous nanofluid between the concentric cylinders. J Comp Theoretical Nanoscience. 2014; 11: 646–654.
8. Sheikholeslami M, Bandpy MG, Ellahi R, Hassan M, Soleimani S. Effects of MHD on Cu-water nanofluid flow and heat transfer by means of CVFEM. J Magn Magn Mater. 2014; 349: 188–200.
9. Sheikholeslami M, Abelman S. Two-phase simulation of nanofluid flow and heat transfer in an annulus in the presence of an axial magnetic field. IEEE Trans Nanotech. 2015; 14: 561–569.
10. Zhang C, Zheng L, Zhang X, Chen G. MHD flow and radiation heat transfer of nanofluids in porous media with variable surface heat flux and chemical reaction. Appl Math Modell. 2015; 39: 165–181.
11. Sheikholeslami M, Ganji DD, Javed MY, Ellahi R. Effect of thermal radiation on magnetohydrodynamics nanofluid flow and heat transfer by means of two phase model. J Magn Magn Mater. 2015; 374: 36–43.
12. Malvandi A, Safaei MR, Kaffash MH, Ganji DD. MHD mixed convection in a vertical annulus filled with Al_2O_3-water nanofluid considering nanoparticle migration. J Magn Magn Mater. 2015; 382: 296–306.
13. Hayat T, Muhammad T, Alsaedi A, Alhuthali MS. Magnetohydrodynamic three-dimensional flow of viscoelastic nanofluid in the presence of nonlinear thermal radiation. J Magn Magn Mater. 2015; 385: 222–229.
14. Chamkha A, Abbasbandy S, Rashad AM. Non-Darcy natural convection flow for non-Newtonian nanofluid over cone saturated in porous medium with uniform heat and volume fraction fluxes. Int J Numer Methods Heat Fluid Flow. 2015; 25: 422–437.
15. Hayat T, Aziz A, Muhammad T, Ahmad B. Influence of magnetic field in three-dimensional flow of couple stress nanofluid over a nonlinearly stretching surface with convective condition. Plos One. 2015; 10: e0145332. doi: 10.1371/journal.pone.0145332 PMID: 26714259
16. Gireesha BJ, Gorla RSR, Mahanthesh B. Effect of suspended nanoparticles on three-dimensional MHD flow, heat and mass transfer of radiating Eyring-Powell fluid over a stretching sheet. J Nanofluids. 2015; 4: 474–484.
17. Lin Y, Zheng L, Zhang X, Ma L, Chen G. MHD pseudo-plastic nanofluid unsteady flow and heat transfer in a finite thin film over stretching surface with internal heat generation. Int J Heat Mass Transfer. 2015; 84: 903–911.
18. Sheikholeslami M, Ellahi R. Electrohydrodynamic nanofluid hydrothermal treatment in an enclosure with sinusoidal upper wall. Appl Sci. 2015; 5: 294–306.
19. Ellahi R, Hassan M, Zeeshan A. Study of natural convection MHD nanofluid by means of single and multi walled carbon nanotubes suspended in a salt water solutions. IEEE Trans Nanotech. 2015; 14: 726–734.
20. Sheikholeslami M, Ellahi R. Three dimensional mesoscopic simulation of magnetic field effect on natural convection of nanofluid. Int J Heat Mass Transfer. 2015; 89: 799–808.
21. Rahman SU, Ellahi R, Nadeem S, Zia QMZ. Simultaneous effects of nanoparticles and slip on Jeffrey fluid through tapered artery with mild stenosis. J Mol Liq. 2016; 218: 484–493.
22. Hsiao KL. Stagnation electrical MHD nanofluid mixed convection with slip boundary on a stretching sheet. Appl Thermal Eng. 2016; 98: 850–861.
23. Hayat T, Aziz A, Muhammad T, Alsaedi A. On magnetohydrodynamic three-dimensional flow of nanofluid over a convectively heated nonlinear stretching surface. Int J Heat Mass Transfer. 2016; 100: 566–572.
24. Malvandi A, Ganji DD, Pop I. Laminar filmwise condensation of nanofluids over a vertical plate considering nanoparticles migration. Appl Thermal Eng. 2016; 100: 979–986.

25. Hayat T, Muhammad T, Shehzad SA, Alsaedi A. On magnetohydrodynamic flow of nanofluid due to a rotating disk with slip effect: A numerical study. Comput Methods Appl Mech Eng. 2017; 315: 467–477.
26. Gupta PS, Gupta AS. Heat and mass transfer on a stretching sheet with suction or blowing. Can J Chem Eng. 1977; 55: 744–746.
27. Vajravelu K. Viscous flow over a nonlinearly stretching sheet. Appl Math Comput. 2001; 124: 281–288.
28. Cortell R. Viscous flow and heat transfer over a nonlinearly stretching sheet. Appl Math Comput. 2007; 184: 864–873.
29. Cortell R. Effects of viscous dissipation and radiation on the thermal boundary layer over a nonlinearly stretching sheet. Phys Lett A. 2008; 372: 631–636.
30. Hayat T, Hussain Q, Javed T. The modified decomposition method and Padé approximants for the MHD flow over a non-linear stretching sheet. Nonlinear Anal-Real World Appl. 2009; 10: 966–973.
31. Rana P, Bhargava R. Flow and heat transfer of a nanofluid over a nonlinearly stretching sheet: A numerical study. Comm Nonlinear Sci Num Simulat. 2012; 17: 212–226.
32. Mukhopadhyay S. Analysis of boundary layer flow over a porous nonlinearly stretching sheet with partial slip at the boundary. Alexandria Eng J. 2013; 52: 563–569.
33. Mustafa M, Khan JA, Hayat T, Alsaedi A. Analytical and numerical solutions for axisymmetric flow of nanofluid due to non-linearly stretching sheet. Int J Non-Linear Mech. 2015; 71: 22–29.
34. Mabood F, Khan WA, Ismail AIM. MHD boundary layer flow and heat transfer of nanofluids over a non-linear stretching sheet: A numerical study. J Magn Magn Mater. 2015; 374: 569–576.
35. Hayat T, Aziz A, Muhammad T, Ahmad B. On magnetohydrodynamic flow of second grade nanofluid over a nonlinear stretching sheet. J Magn Magn Mater. 2016; 408: 99–106.
36. Kothandapani M, Srinivas S. Peristaltic transport of a Jeffrey fluid under the effect of magnetic field in an asymmetric channel. Int J Non-Linear Mech. 2008; 43: 915–924.
37. Alsaedi A, Iqbal Z, Mustafa M, Hayat T. Exact solutions for the magnetohydrodynamic flow of a Jeffrey fluid with convective boundary conditions and chemical reaction. Z Naturforsch A. 2012; 67a: 517–524.
38. Turkyilmazoglu M, Pop I. Exact analytical solutions for the flow and heat transfer near the stagnation point on a stretching/shrinking sheet in a Jeffrey fluid. Int J Heat Mass Transfer. 2013; 57: 82–88.
39. Hayat T, Muhammad T, Shehzad SA, Alsaedi A. A mathematical study for three-dimensional boundary layer flow of Jeffrey nanofluid. Z Naturforsch A. 2015; 70a: 225–233.
40. Hayat T, Qayyum S, Imtiaz M, Alsaedi A. Impact of Cattaneo-Christov heat flux in Jeffrey fluid flow with homogeneous-heterogeneous reactions. Plos One. 2016; 11: e0148662. doi: 10.1371/journal.pone.0148662 PMID: 26859675
41. Hayat T, Abbas T, Ayub M, Muhammad T, Alsaedi A. On squeezed flow of Jeffrey nanofluid between two parallel disks. Appl Sci. 2016; 6: 346.
42. Gao ZK, Fang PC, Ding MS, Jin ND. Multivariate weighted complex network analysis for characterizing nonlinear dynamic behavior in two-phase flow. Exp Therm Fluid Sci. 2015; 60: 157–164.
43. Gao ZK, Yang YX, Fang PC, Jin ND, Xia CY, Hu LD. Multi-frequency complex network from time series for uncovering oil-water flow structure. Sci Rep. 2015; 5: 8222. doi: 10.1038/srep08222 PMID: 25649900
44. Gao ZK, Yang YX, Zhai LS, Ding MS, Jin ND. Characterizing slug to churn flow transition by using multivariate pseudo Wigner distribution and multivariate multiscale entropy. Chem Eng J. 2016; 291: 74–81.
45. Gao Z, Yang Y, Zhai L, Jin N, Chen G. A four-sector conductance method for measuring and characterizing low-velocity oil-water two-phase flows. IEEE Trans Instrumentation Measurement. 2016; 65: 1690–1697.
46. Makinde OD, Aziz A. Boundary layer flow of a nanofluid past a stretching sheet with a convective boundary condition. Int J Thermal Sci. 2011; 50: 1326–1332.
47. Hayat T, Muhammad T, Shehzad SA, Alsaedi A. An analytical solution for magnetohydrodynamic Oldroyd-B nanofluid flow induced by a stretching sheet with heat generation/absorption. Int J Thermal Sci. 2017; 111: 274–288.
48. Kuznetsov AV, Nield DA. Natural convective boundary-layer flow of a nanofluid past a vertical plate: A revised model. Int J Thermal Sci. 2014; 77: 126–129.
49. Hayat T, Muhammad T, Shehzad SA, Alsaedi A. On three-dimensional boundary layer flow of Sisko nanofluid with magnetic field effects. Adv Powder Tech. 2016; 27: 504–512.
50. Liao SJ. On the homotopy analysis method for nonlinear problems. Appl Math Comput. 2004; 147: 499–513.
51. Dehghan M, Manafian J, Saadatmandi A. Solving nonlinear fractional partial differential equations using the homotopy analysis method. Numer Meth Partial Diff Eq. 2010; 26: 448–479.

52. Ellahi R. The effects of MHD and temperature dependent viscosity on the flow of non-Newtonian nanofluid in a pipe: Analytical solutions. Appl Math Model. 2013; 37: 1451–1467.

53. Malvandi A, Hedayati F, Domairry G. Stagnation point flow of a nanofluid toward an exponentially stretching sheet with nonuniform heat generation/absorption. J Thermodynamics. 2013; 2013: 764827.

54. Abbasbandy S, Hayat T, Alsaedi A, Rashidi MM. Numerical and analytical solutions for Falkner-Skan flow of MHD Oldroyd-B fluid. Int J Numer Methods Heat Fluid Flow. 2014; 24: 390–401.

55. Ellahi R, Hassan M, Zeeshan A. Shape effects of nanosize particles in Cu-H_2O nanofluid on entropy generation. Int J Heat Mass Transfer. 2015; 81: 449–456.

56. Sui J, Zheng L, Zhang X, Chen G. Mixed convection heat transfer in power law fluids over a moving conveyor along an inclined plate. Int J Heat Mass Transfer. 2015; 85: 1023–1033.

57. Turkyilmazoglu M. An effective approach for evaluation of the optimal convergence control parameter in the homotopy analysis method. Filomat. 2016; 30: 1633–1650.

58. Hayat T, Hussain Z, Muhammad T, Alsaedi A. Effects of homogeneous and heterogeneous reactions in flow of nanofluids over a nonlinear stretching surface with variable surface thickness. J Mol Liq. 2016; 221: 1121–1127.

59. Hayat T, Muhammad T, Alsaedi A, Mustafa M. A comparative study for flow of viscoelastic fluids with Cattaneo-Christov heat flux. Plos One. 2016; 11: e0155185. doi: 10.1371/journal.pone.0155185 PMID: 27176779

60. Hayat T, Waqas M, Shehzad SA, Alsaedi A. Mixed convection flow of viscoelastic nanofluid by a cylinder with variable thermal conductivity and heat source/sink. Int J Numer Methods Heat Fluid Flow. 2016; 26: 214–234.